ISSS Journal of Micro and Smart Systems (2022) 11:317–328
https://doi.org/10.1007/s41683-021-00088-z

REVIEW PAPER

Magnetically enhanced photoconductive high voltage control

G. J. Monkman[1] · D. Sindersberger[1] · N. Prem[1]

Received: 19 August 2021 / Revised: 23 October 2021 / Accepted: 12 December 2021 / Published online: 9 March 2022

Abstract
The recent surge of interest in electrostatic actuators, particularly for soft robotic applications, has placed increasing demands on high voltage control technology. In this respect, optoelectronic bidirectional switching and analogue regulation of high voltages is becoming increasingly important. One common problem is the leakage current due to dark resistance of the material or device used. Another is the physical size of such elements. However, their ability to provide galvanic separation makes them a very attractive alternative to conventional (wired) semiconductor elements. This paper gives an overview of available methods and devices before introducing a concept based on the combination of photoresistive and magnetoresistive effects in Gallium Arsenide that are potentially applicable to other semiconductor materials.

Keywords High voltage actuators · Opto-sensors · Photoconduction · GaAs · Magnetoresistance · Soft robotics

Introduction

Most electrostatically driven actuators require electric field strengths of up to 4000 V/mm. Ferroelectric (piezoelectric and electrostrictive) (Waanders 1991), dielectric (elastomer) actuators (Thummala et al. 2012) and electroadhesors (Monkman 2000) are all of increasing interest in soft robotics (Kim and Tadokoro 2007). In such applications, the actuators are part of the robotic structure or must be embedded within a polymer matrix (Zhu et al. 2016). It is convenient, if not essential, to integrate the high voltage control device within the same matrix. In addition, galvanic separation is extremely desirable. In the reverse case, systems exploiting the movement of dielectric elastomer actuators to carry out high voltage switching, logic processes and even oscillation have been built (Henke et al. 2017). Most rely on the application of force generated by an electroactive or magnetoactive device against a piezoresistive polymer for current control (Henke and Gerlach 2016).

Intrinsic optoisolation is a distinct advantage offered by photonically, rather than electrically, driven devices. The possibility of small-scale fabrication is also essential, and the ability to be operated bidirectionally is highly desirable. Using silicone technology, suitable photodiodes are commercially available but are unidirectional because of the PN-junction and are currently only available in forms unsuitable for miniaturization (Opto-150 2021). Amorphous silicon is known for its ability to handle high voltages and by means of chemical vapour deposition devices suitable for use with dielectric elastomer actuators have been built (Lacour et al. 2003; Gillespie et al. 2019).

This paper discusses a range of techniques and devices capable of controlling high voltages before demonstrating how the basic photoresistive effect applicable to most direct band gap semiconductors, including Gallium Arsenide (GaAs), can be used for such purposes and greatly enhanced through an additional magnetoresistive effect. Further details of practical design considerations, particularly with respect to frequency response are also discussed.

Photoelectric sensors

The photoelectric effect relies on the work function Φ of materials which expel electrons when they are struck by photons of a high enough energy (Wolfson and Pasachoff 1999). When a negatively charged surface (cathode) of such a material is held in proximity to a smaller, positively charged anode (in vacuum), electrons expelled from the

✉ G. J. Monkman
gareth.monkman@oth-regensburg.de

[1] Mechatronics Research Unit, OTH Regensburg, Seybothstr. 2, 93053 Regensburg, Germany

cathode by photon impact will be attracted to the anode. The effective kinetic energy of a photon is inversely proportional to its wavelength λ, thus:

$$\lambda = \frac{hc}{q\Phi} \tag{1}$$

where h is 6.63×10^{-34} Js, $c = 2.998 \times 10^{8}$ m/s and $q = 1.6 \times 10^{-19}$ C.

Table 1 shows typical work functions and their corresponding maximum operating wavelengths for some basic photocathode materials. The majority comprise polycrystalline alkali metals. For a more comprehensive collection, the reader is referred to texts with more extensive coverage (Tipler and Llewellyn 1999; Halas and Durakiewicz 1998). In the latter case, the measured work functions differ slightly from those calculated but all are within 5%.

In some cases, these values may differ for particular crystal structures, for example that of silver can vary between 4.26 eV and 4.81 eV (Dweydari and Mee 1975).

Sensors of this type, capable of working at up to 2500 V with an almost infinitely high dark resistance, are commercially available. Furthermore, they are controllable in an analogue manner with visible illumination and capable of passing currents of up to 30 μA.

The voltage dependent flow of dark current through a miniature vacuum photodiode (Hamamtsu, R727) is shown in Fig. 1. To around 2500 V, there is very little voltage dependency. Thereafter the dark current rises rapidly making it of little use at potentials higher than 2500 V. Physical size and cost of currently available sensors may also be a problem. However, there is no scientific reason why such devices could not be cost effectively manufactured at much smaller scales.

The electrical breakdown strength of dry air is nominally 3000 V/mm at distances above 1 mm (Rigden 1996). However, at much lower dimensions, and particularly at low pressures (or in vacuum) this figure rises dramatically (Paschen 1889). Good use is made of this phenomenon in field emitters where electrical field strengths of up to 50 kV/mm are not uncommon. Under illumination, the resistivity of cathodes fabricated from intrinsically doped n-type and p-type silicon fall to as low as 0.005 Ωm and 1 to 10 Ωcm, respectively (Langer et al. 2014). The reduced resistivity can be evoked through pulsed laser irradiation of the silicon surface resulting in current flows in the nA to low μA ranges (Langer et al. 2016). However, at larger scales and normal atmospheric pressure, implementation becomes a problem.

For much higher voltages, gas filled thyratrons and trigatrons were the traditional switching devices before the advent of semiconductor thyristors. Triggering is usually achieved by means of a voltage applied to a grid. This ionizes part of the gas, which results in an avalanche effect leading to total ionization that in turn results in a drastic decrease in resistance between the anode and cathode (Howatson 1965). Like thyristors, it is impossible to switch the device off my means of the grid or gate electrode. Furthermore, hold-on currents tend to be relatively large thus reducing their potential for switching high voltages at low currents. An alternative way of triggering is by ultraviolet light as is the case with flame detectors. However, the same problem exists in that the voltage supply to the device must be periodically removed as the gas remains ionized after removal of the UV radiation. Consequently, such devices are of limited use in the context of this paper and will not be discussed further.

Other potential devices include semiconductor PIN and avalanche diodes (Myres 1980). Unfortunately, all such components suffer from the existence of PN-junctions, which are not capable of bidirectional operation with a single device and are sensitive to electrical breakdown potentially resulting in permanent damage.

Direct band-gap semiconductor photoconductors

In all direct band gap semiconductors (InSb, GaP, CdS, GaAs etc.) the conduction band minimum corresponds almost directly with the valence band maximum as can be seen in the left-hand side of Fig. 2 (Ashby et al. 2015). Unfortunately, the most common semiconductor, silicon is not of this form as shown at the right-hand side of Fig. 2.

Table 1 Photocathode characteristics

Photocathode	Work function Φ (eV)	Wavelength λ (nm)	References
Silver (Ag)	4.26	292	Hölzl and Schulte (1979)
Aluminium (Al)	4.06–4.28	290–305	CRC (2008)
Cesium (Cs)	2.14	581	Halas and Durakiewicz (1998)
Copper (Cu)	4.65–4.81	258–267	CRC (2008)
Potassium (K)	2.30	540	Halas and Durakiewicz (1998)
Sodium (Na)	2.75	452	Halas and Durakiewicz (1998)
Nickel (Ni)	5.05–5.35	232–246	CRC (2008)
Silicon (Si)	4.6–4.85	256–270	CRC (2008)

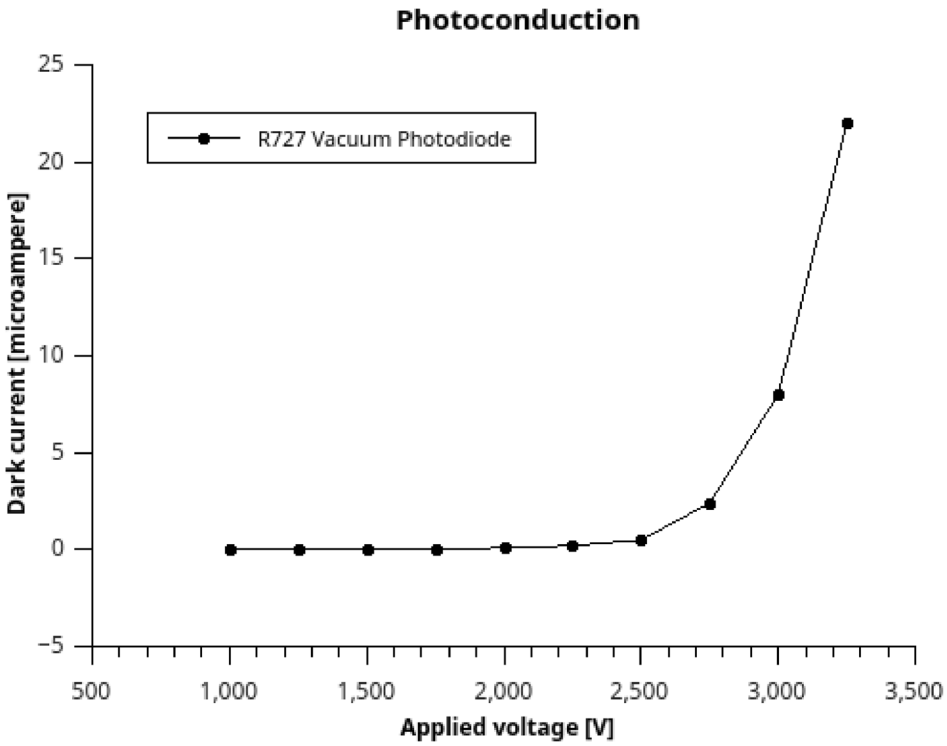

Fig. 1 Vacuum Photodiode dark current [μA] for applied voltage [V]

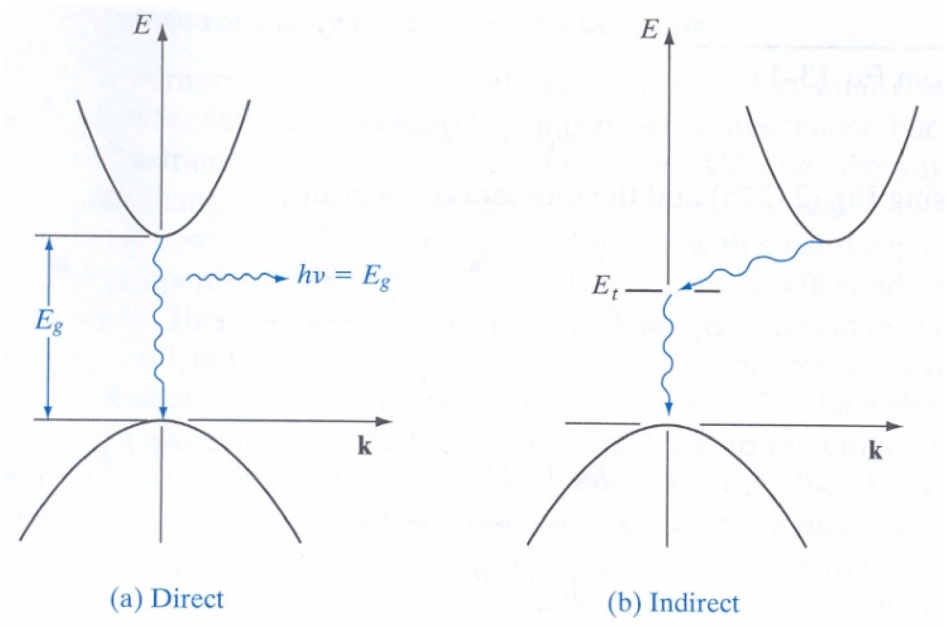

Fig. 2 **a** direct-transition and **b** indirect-transition semiconductors (courtesy Ohio State University) (http://www2.ece.ohio-state.edu/~lu/ECE331_Wi06_lec_10.pdf)

Due to thermal problems, optically controlled semiconductors for the high voltage switching of Pockel's cells using intrinsic silicon were found to be inferior to those made from GaAs (Mourou and Knox 1979).

When direct band gap semiconductor materials are used as photo-conductors, incident light causes the generation and recombination of charge carriers with electron mobility μ. This leads to a decrease in electrical resistance over the material surface. The carrier transition time between electrical contacts is given by expression (2).

$$t_d = \frac{l^2}{\mu V} \tag{2}$$

where

$$\mu = \mu_e\left(1 + \frac{\mu_h}{\mu_e}\right) \tag{3}$$

From expression (2), a strong voltage dependency is clear. For most photoconductive materials, and particularly Cadmium sulphide (CdS) commonly used in inexpensive LDRs, this can be a problem. A rapid response time demands a relatively high voltage.

Given an electron lifetime τ (hole lifetimes are comparatively short for CdS and so can be neglected), electrons flow over the distance l between two terminals due to an applied voltage V. The electron flow increases by a factor A, given by the ratio between the number of electrons passing between the contacts and the number of photonically generated electrons, when the CdS is illuminated (Gardner 1994).

$$A = \frac{\mu\tau V}{l^2} \tag{4}$$

Clearly, A is not only light dependant but also strongly voltage dependant. This is the main reason why most LDR devices are usable only up to about 200 V.

Although there are some LDR devices capable of withstanding over 1000 V their characteristics change nonlinearly above a certain voltage level as shown in Fig. 3. Consequently, many such devices having a dark resistance of over 100 MΩ at low voltages exhibit dark resistances some 1000 times lower at higher potentials. Furthermore, as higher currents flow, due to the relatively low dark resistance, the unilluminated underside of the material acts as shunt resistance leading to thermal effects which further reduce the resistance causing excessive current flow (Bar-Lev 1979).

Figure 3 shows three example curves for commonly available LDRs. Their respective manufacturer's data are shown in Table 2. The NSL-4960 (Silonex) and the PDV-P5003 (Advances Photonics) are Cadmium Sulphide, while the U-116033 (Perkin Elmer) is Cadmium Sulphide Selenide (Perkin Elmer 2001).

Despite manufacturers designated operating voltages of under 320 V, samples tested exhibited relatively consistent high dark resistance to about 1000 V. For most such devices, a temperature dependency of about 0.35%/°C resistance change may be observed.

GaAs photoconductive devices

Gallium Arsenide (GaAs) is a direct band gap semiconductor known to have optical sensitivity and undoped GaAs has the ability to withstand high electric field strengths (Solymar and Walsh 1993; Hrivnak 1984). The use of GaAs for the switching of high voltages was first mentioned in 1989, though with Schottky contacts (Wiener et al. 1989). Originally conceived for the control of electrorheological fluid based tactile displays, where large arrays of small elements are required, GaAs was employed

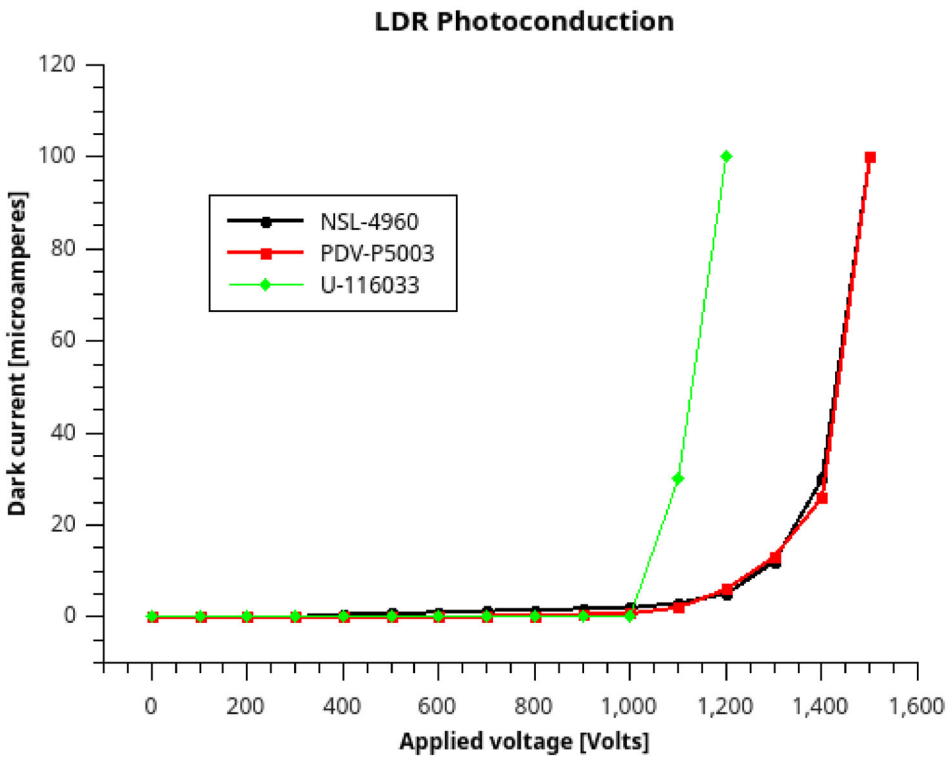

Fig. 3 CdS and CdSSe LDR dark current [μA] for applied voltage [V]

Table 2 Characteristics of 3 selected LDR devices

Device	Material	λ (nm)	τ_{on} (ms)	τ_{off} (ms)	V (max) (V)	R_d (min) (MΩ)
NSL-4960	CdS	515	30	–	320	1
PDV-P5003	Cds	520	25	100	350	1
U-116033	CdSSe	550	30	25	400	1.1

as an optical high voltage switch without PN-junctions (Monkman et al. 2003). The extremely high dark resistance of semi-insulating GaAs and low voltage dependency means that only the surface of the material is brought into conduction.

Various sizes of semi-insulating GaAs (III/V-Reclaim 181/04-1) wafer were cut (along and orthogonal to the crystal axes) and tested at voltages up to 10 kV. Electrical contacts were made using non-Schottky metal–semiconductor connections by means of electrically conducting paint. This may appear somewhat unscientific, but the conventional means of indium soldering or SMD contacting using chromium gives rise to diffusion within the GaAs resulting in unwanted PN junctions, which often suffer from irreversible damage due to electrical breakdown at high voltages. Other researchers (Wiener et al. 1989) have also observed the necessity for standard ohmic contact procedures.

The configuration described above is illustrated in Fig. 4. To control higher voltages, the dimensions may simply be scaled up. Figure 5 shows the characteristic dark current curves for 2 mm square and 4 mm square elements. From this, it can be seen that the asymptotic break point for 2 mm devices lies around 2500 V, while for 4 mm elements the voltage break point is roughly double. Figure 5 reveals a sheet resistance of 375MΩ/□ at 3 kV for the 2 × 2 mm elements and at 6 kV for the 4 × 4 mm elements. At voltages under 2 kV sheet resistance in the GΩ/□ to TΩ/□ can be seen.

Fitting an exponential growth curve (5) to the data from Fig. 5, and ignoring small offsets reveals a dark current proportional to the exponent and the applied voltage and a constant β, which is related to the area of the element.

$$I_d = \alpha e^{V/\beta} \tag{5}$$

The constant α is dependent on other factors such as magnetic field strength, which will now be considered.

Magnetoresistance

Many semiconductors exhibit Hall Effect, and GaAs is no exception (Kemei et al. 2012). The application of a magnetic flux $\boldsymbol{B}$ during current flow of density $\boldsymbol{J}$ is usually used to generate an electric field $\boldsymbol{E}$.

For Hall effect (6), all three fields i.e. J_{xx}, E_{yy} and B_{zz}, are orthogonal.

$$J_{xx}B_{zz} = -nqE_{yy} \tag{6}$$

However, in this case a voltage is applied for which the current flow is in the same direction, and only the magnetic flux is applied at right angles to the device. This magnetoresistive effect has also been observed in doped GaAs MOSFET devices where the greater the magnetic flux density, the higher the effective electrical resistance (Look 1990).

Figure 6 shows the resistance of a 4 × 4 mm undoped GaAs device at room temperature (295 K) for a range of magnetic flux densities from 0 to 0.27 Tesla. The magnetic

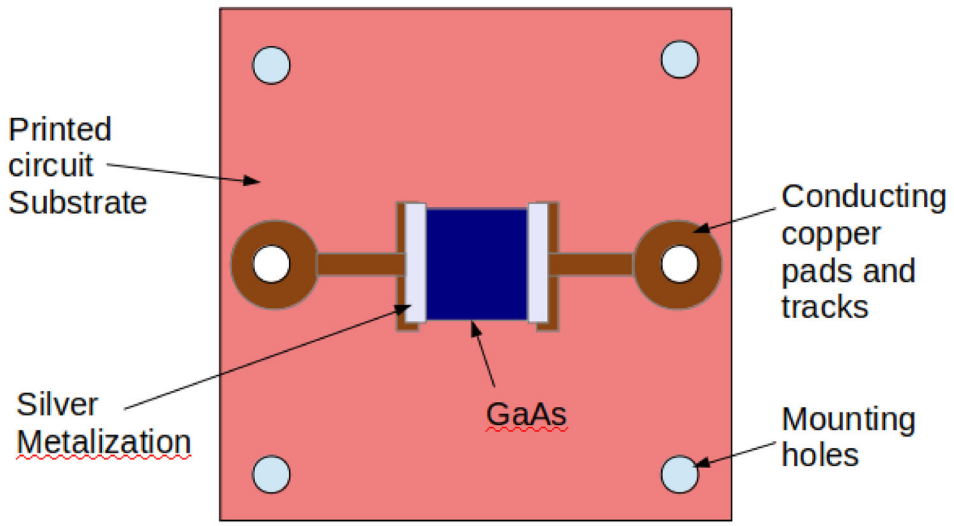

Fig. 4 Basic mounting of GaAs element

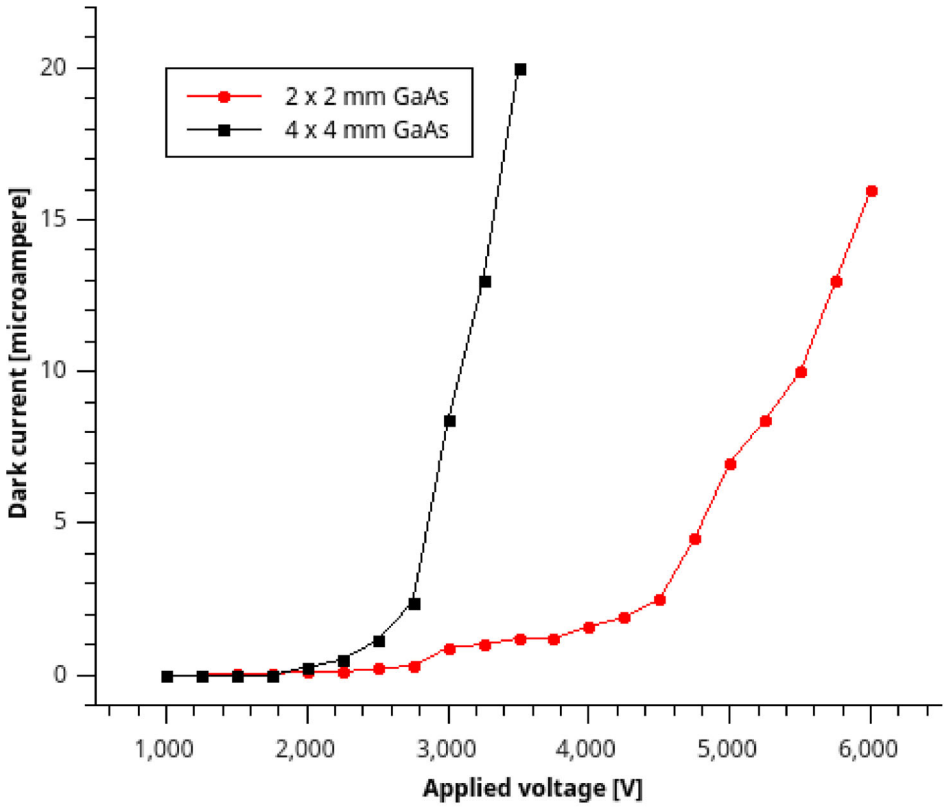

Fig. 5 Dark current for 2 by 2 mm and 4 by 4 mm GaAs elements

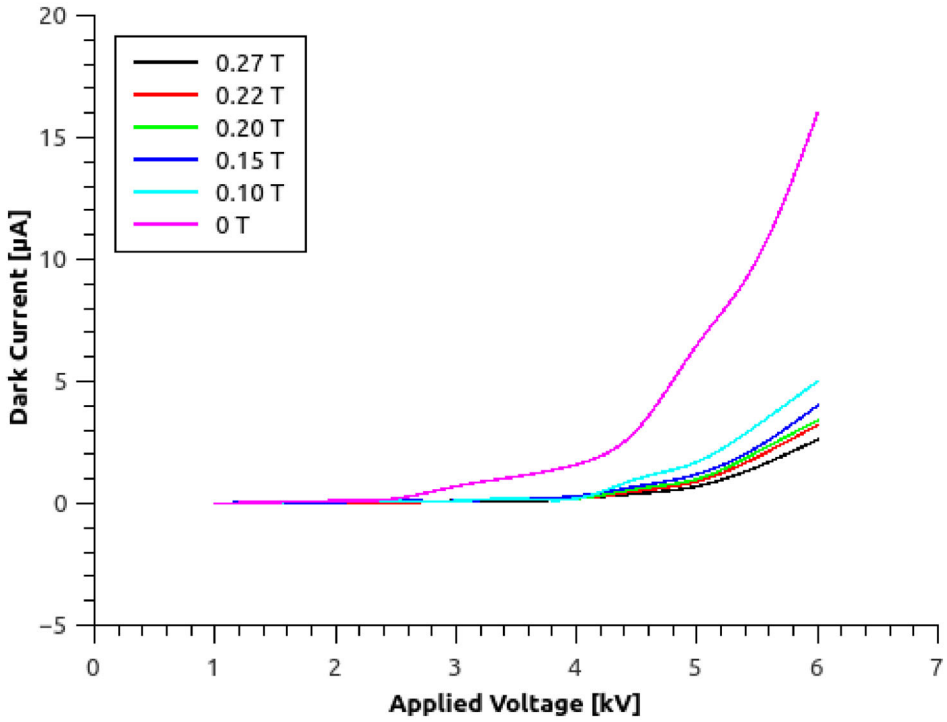

Fig. 6 Dark current for GaAs with and without magnetic field

field was provided by 10 mm diameter permanent magnets mounted behind the GaAs and the flux density measured on the surface of the GaAs using a Gaussmeter (Lakeshore 455 DSP). The polarity of the magnetic field had no discernible influence on the effect.

Below 1.5 kV (2 kV in the cases of 0.22 and 0.27 Tesla applied magnetic flux densities), the resistance was extremely high and consequent current flow almost zero.

Dividing the applied voltage by the dark current in Fig. 6 gives the dark resistance. Fitting exponential growth functions to this and applying expression (5) reveals a strong influence on α from the magnetic flux density.

Magnetoresistance is defined as the change in electrical resistance denoted by a magnetoresistive factor $\Delta R/R_0$ (Hirota et al. 2002) which is proportional to the square of the product of electron mobility μ and magnetic flux density B (Hishiyama et al. 2016).

$$\delta_B = \frac{\Delta R}{R_0} = \frac{R_B - R_0}{R_0} \propto \mu^2 B^2 \tag{7}$$

However, to be exact, expression (7) is only valid for very small changes in resistance. A more accurate factor would be that given by Eq. (8).

$$\int_{R_0}^{R} \frac{1}{R} dR = ln\left(\frac{R}{R_0}\right) = ln(1 + \delta_B) \tag{8}$$

This can be verified by recourse to the values shown in Fig. 6. Using expression (8) the factor over a large range will now be the same as the sum of that resulting from smaller increments. With (7) it is not.

Look (1990) is a little more precise and gives the resistance as a function of magnetic flux density (9).

$$R(B) = R_0\left(1 + \mu^2 B^2\right) \tag{9}$$

For small values of μ^2 B^2 Eq. (9) can also be expressed in exponential form (10).

$$R(B) = R_0 e^{\mu^2 B^2} \tag{10}$$

That the dark resistance is both a function of applied voltage and magnetic flux density is clearly be seen in Fig. 6. Here it can also be seen that δ_B is a nonlinear function of magnetic field strength (assuming unity magnetic relative permeability μ_r). Closer observation of Fig. 6 reveals an exponential decay function between α and magnetic flux density B.

$$I_d = e^{-B^2/\gamma} e^{V/\beta} = e^{V/\beta - B^2/\gamma} \tag{11}$$

Combining both effects in Eq. (11) gives the general dark current characteristics, where γ is a constant related to the magnetoresistance of the element.

Figure 7 shows spectral measurements over the range 400 to 900 nm. These are typical for GaAs and very similar to those from other authors (Salzberger et al. 2017). No discernible differences were observed between spectral plots with or without an applied magnetic field.

These are similar to absorption curves in crystalline GaAs (400–860 nm) intended for photovoltaic purposes (Eyderman et al. 2014). GaAs has a band gap energy of 1.42 at 300 K which limits the wavelength to around 900 nm anyway.

Test and evaluation

The complete configuration, depicted in exploded view form in Fig. 8, comprises a permanent magnet (or electromagnet), the GaAs element and an LED mounted in a lightproof housing.

During illumination, photoconduction dominates making measurable effects of the magnetic field negligible. However, just above the conduction threshold, the application of the magnetic field can be used to quench conduction and so provide magnetic class-D modulation of the device if required.

As shown in Fig. 7, GaAs is sensitive at the red/infrared end of the electromagnetic spectrum and illumination wavelengths between 200 and 850 nm are usually suitable (Pesavento 1987).

A 640 nm LED was characterized using a 9.5 mm diameter silicon photodiode power sensor (Thor Labs S130VC). Figure 9 shows the LED optical output power for given electrical input power. Contrary to most of the GaAs curves, the graph shown in Fig. 9 is represented by a second-order polynomial function (12).

$$P_0 = 0.014P_i - 3.2 \cdot 10^{-5} P_i^2 \tag{12}$$

Figure 10 shows the electrical resistances of the device under different levels of illumination. The values given are LED input powers. Below 1 kV in Fig. 10a and under 1.5 kV in Fig. 10b, the resistances shown are too high to be presented on a reasonable graphical scale and so have been omitted.

In these measurements, the increase in dark resistance approached a plateau over 0.2 Tesla axial field. This is in line with other researchers findings (Viana et al. 2012). For a transverse magnetic field, the effects were found to be less pronounced. Like all semiconductors, many electrical characteristics of GaAs are temperature dependent and this effect results in a reduction in electrical resistance at higher temperatures and a peak for a given flux density (Viana et al. 2012).

Only at relatively low levels of illumination, can the effects of an applied magnetic field be seen. At higher levels, the characteristics are very similar regardless of the magnetic field strength. Consequently, in GaAs, photoconductive effects dominate over magnetoresistive effects.

Response time

The rate at which the conductivity of the device increases during illumination is given by the difference between the

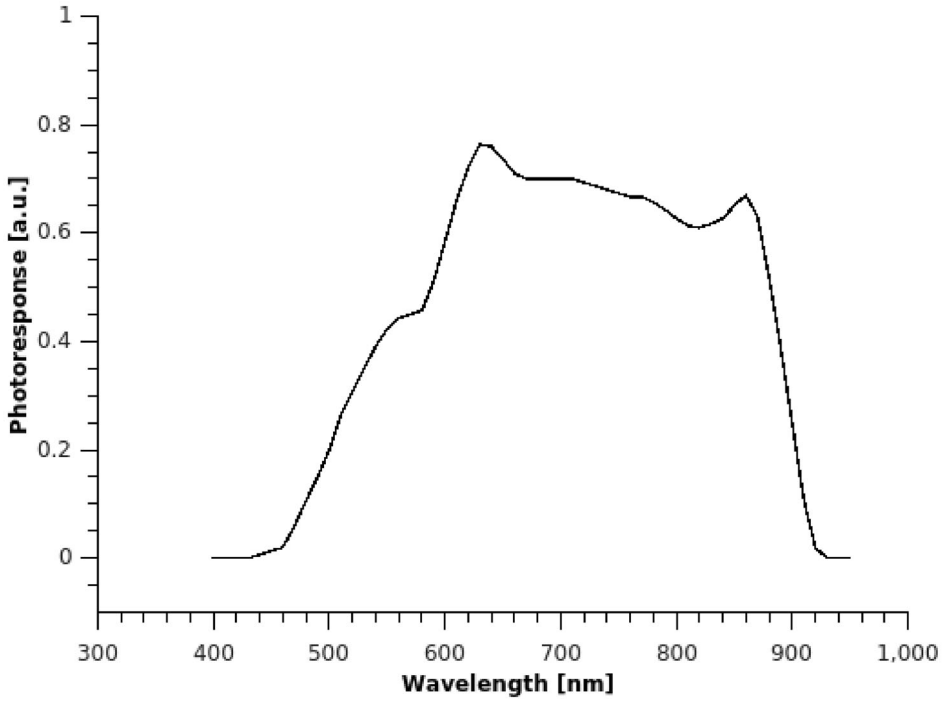

Fig. 7 Photoresponse (arbitrary units) against wavelength [nm] for GaAs

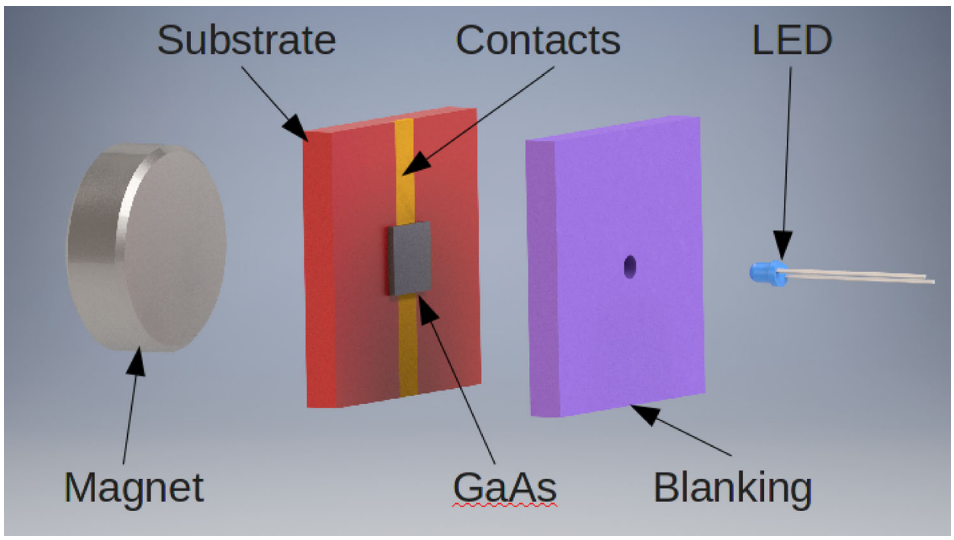

Fig. 8 Complete magneto-opto-electrical test configuration

rates at which charge carriers are created and recombine, and vice-verse for the carrier decay rate. For GaAs the electron and hole mobilities are $\mu_e = 0.85\ \mathrm{m^2\ V^{-1}\ s^{-1}}$ and $\mu_h = 0.045\ \mathrm{m^2\ V^{-1}\ s^{-1}}$, respectively (Ashby et al. 2015).

When direct band gap semiconductor materials are used as photo-conductors, incident light causes the generation and recombination of charge carriers with electron mobility μ. This leads to a decrease in electrical resistance over the material surface. The carrier transition time between electrical contacts is given by expression (13).

$$t_d = \frac{l^2}{\mu V} \tag{13}$$

where

$$\mu = \mu_e \left(1 + \frac{\mu_h}{\mu_e}\right) \tag{14}$$

Consequently, from (13) the carrier transition time over a 2 mm GaAs surface at 2000 Volts should be in the region of 2 ns. However, this does not take into account the capacitance of the device and its respective electrical time constant.

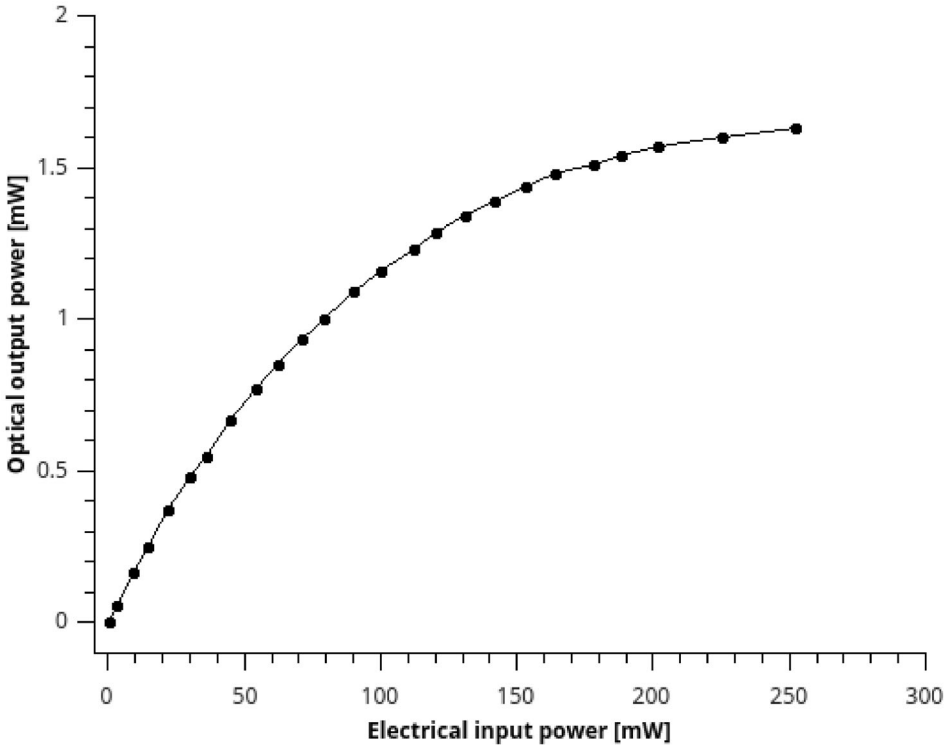

Fig. 9 Optical output power as a function of electrical input power

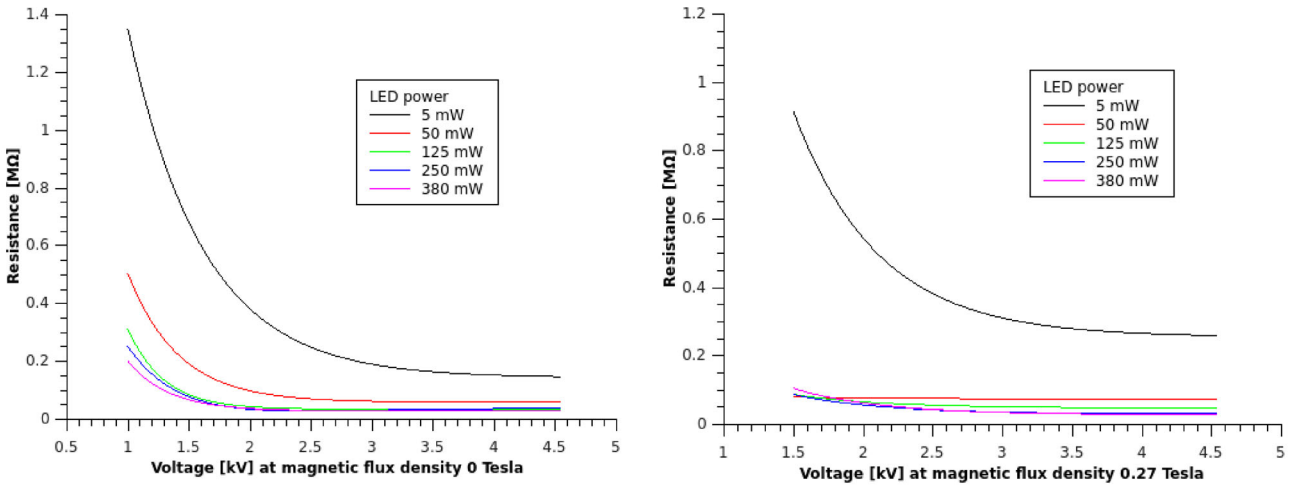

Fig. 10 Illuminated GaAs **a** without magnetic field, **b** with 0.27 T magnetic flux density

Many optical functions of GaAs have been determined by two-channel polarization modulation ellipsometry. At a wavelength of 620 nm (2 eV) GaAs (111) and (100) has a refractive index $n = 3.873$ and an absorption coefficient (attenuation constant) $\alpha = 47{,}990\ \mathrm{cm}^{-1}$ (Jellison 1992). The relative permittivity is the square of the refractive index so $\varepsilon_r = 15.00$.

According to the Beer-Lambert Law, the penetration depth (skin depth) of electromagnetic radiation is defined as the depth at which the intensity of the radiation $I(z)$ inside the material falls to $1/e$ (about 37%) of its original value I_0.

$$I(z) = I_0 e^{-\alpha z} \tag{15}$$

The penetration depth is the reciprocal of the attenuation constant ($1/\alpha$) which is 0.208 µm for $\alpha = 4{,}799{,}000\ \mathrm{m}^{-1}$. This means that almost all of the 625 µm thick GaAs wafer contributes to the capacitance which, given $\varepsilon_r = 15.00$, equates to about 0.083 pF.

The electrical time constant is simply given by the product of capacitance and resistance $\tau = CR$. However,

the rate at which a given resistance is reached depends on the carrier transition time. With an instantaneous illumination, a resistance of 2 MΩ should be reached within 2 ns.

However, the capacitance dominates and so the resulting rise time is given almost exclusively by the simple CR time constant (16).

$$\tau_{on} = CR = 166 \text{ ns} \tag{16}$$

When the illumination ceases, the dark resistance of 4 GΩ is also reached in just over 2 ns giving the decay time in expression (15).

$$\tau_{off} = CR = 332\ \mu S \tag{17}$$

Tests carried out on 2 mm by 2 mm GaAs elements, switched at 2000 Volts reveal slightly longer rise times, but comparable decay times (Zappa et al. 2004). This generally in line with other findings which claim switching pulse width typically 10 µs to 10 ms (Mourou 1980).

Current carrying capability

With a density of 5.3267 g/cm^2 (Sze 1981), the 2 mm square and 4 mm square GaAs elements used in this work have masses of 0.013 g and 0.051 g, respectively. This presents little difficulty for the integration of a plurality of such devices in almost any system. Although not intended for large current applications, with all such embedded devices, heat generation in an important factor.

It can be observed from Fig. 10 that, under illumination and an applied magnetic field, the resistance rapidly sinks to a few hundred kΩ. With respect to expression (1), the penetration depth of 0.208 µm means a 2 by 2 mm area GaAs element has an effective cross-sectional area of 416 µm^2.

$$\rho = \frac{RA}{l} \tag{18}$$

According to (18), the effective electrical resistivity during conduction is 0.0208 Ωm, which is comparable to that of Germanium (Hrivnak 1984).

Although the resistivity characteristics of doped GaAs can vary around the room temperature region (Wang et al. 2011), like other semiconductors such as Germanium and Silicon, GaAs devices have a negative temperature coefficient (Viana et al. 2012). However, the application of a magnetic field mitigates this process somewhat, as the Hall mobility in GaAs reduces with increasing temperature (Blakemore 1982).

In many miniaturized applications, the weak point is not the element itself but the interconnections, particularly where metallization is involved. A current density of 2000 MA/m^2 in copper and silver tracks used in hybrid thin film devices leads to a 16 °C temperature increase in normal atmosphere (Kilgore et al. 2005). This equates to a maximum current of around 80 mA but such a temperature rise would be undesirable, particularly in polymeric embedded systems.

Without embarking on a thermodynamic analysis, it should be clear that for most high voltage devices, such current densities are unrealistic. This is particularly so with respect to integration into miniature or soft robotic devices. To compare with commercially available high voltage optical diodes, a maximum power dissipation of 1.25 Watts at 15 kV (Opto-150 2021) means a maximum current of 83 µA. The GaAs devices discussed here can easily achieve similar current levels.

Conclusions

This work has reviewed an important aspect of high voltage control, which is of growing interest in many scientific areas including that of smart materials, systems and devices. Conventional photoelectric and photoconductive devices have been examined and their relevance to such applications considered.

Finally, the electrical resistance of undoped semi-insulating GaAs has been shown to be a function of applied voltage, magnetic field and optical illumination. All three effects have been measured individually and devices characterized. As a result, optically isolated analogue control of very high voltages can be achieved in single GaAs semiconductor elements. The lack of PN-junctions ensures electrical robustness whilst allowing bidirectional control in a single element. The comparably high dark resistance of GaAs can be further increased through the application of a magnetic field, which can easily be achieved using small permanent magnets rather than large and bulky coils. Consequently, such elements can be fabricated at small scales making them suitable for direct integration, together with photonic sources such as LED or laser emitters. Alternatively, the optical signals can be delivered by means of fibre optic links thus ensuring galvanic isolation and additional electromagnetic compatibility.

Application examples include the control of electroactive polymers and electroadhesors in soft robotics, electrorheological fluids, piezoelectric and electrostrictive elements used in tactile displays and other sub-miniature mechanisms. The control of conventional electro-optic devices such as Pockel's cells, photomultipliers are also of interest.

Acknowledgements The authors would like to express their thanks to the German Ministry for Research and Education (BMBF) for their support in the HASASEM project (Grant 01IRA14D) and German

Research Federation (DFG) for financial support within the SPP1681 (Grant MO 2196/2-1) research program.

Funding Open Access funding enabled and organized by Projekt DEAL.

References

Ashby M, Davies T, Gorsse S (2015) The CES EduPack DB for bulk functional materials. Granta teaching resources, January 2015. https://www.researchgate.net/publication/281712335. Accessed 12 Aug 2021

Bar-Lev A (1979) Semiconductors and electronic devices. Prentice-Hall

Blakemore JS (1982) Semiconducting and other major properties of gallium arsenide. J Appl Phys 53:R123–R181. https://doi.org/10.1063/1.331665

CRC (2008) Handbook of chemistry and physics. p 12–114

Dweydari AW, Mee CHB (1975) Work function measurements on (100) and (110) surfaces of silver. Phys Stat Sol (a) 27:223

Eyderman S, Deinega A, John S (2014). Near perfect solar absorption in ultra-thin-film GaAs photonic crystals. J Mater Chem A, Issue 3

Gardner JW (1994) Microsensors: principles and applications. Wiley, Chichester

Gillespie C, Marzo A, Scarpa F, Rossiter J, Conn AT (2019) High-voltage photonic switching of dielectric elastomers with amorphous silicon thin-films. Proc. International Society for Optical Engineering 10966 Smart Structures. https://doi.org/10.1117/12.2514558

Halas S, Durakiewicz T (1998) Work functions of elements expressed in terms of the Fermi energy and the density of free electrons. J Phys: Condens Matter 10:10815–10826

Henke M, Schlatter S, Anderson IA (2017) Soft dielectric elastomer oscillators driving bioinspired robots. Soft Rob. https://doi.org/10.1089/soro.2017.0022

Henke M, Gerlach G (2016) A multi-layered variable stiffness device based on smart form closure actuators. J Intell Mater Syst Struct 27:375–383. doi:https://doi.org/10.1177/1045389X15577645

Hirota H, Sakakima H, Inomata K (2002) Giant magneto-resistance devices. Springer. ISBN 978-3-662-04777-4

Hishiyama Y, Kaburagi YK, Inagaki M (2016) Materials science and engineering of carbon characterization: Chapter 9 Magnetoresistance. Butterworth-Heinemann. https://doi.org/10.1016/B978-0-12-805256-3.00009-X.

Hölzl J, Schulte FK, Wagner H (1979) Solid surface physics. Springer, Berlin

Howatson AM (1965) An introduction to gas discharges. Pergamon, Oxford

Hrivnak L (1984) Semi-insulating GaAs. Czech J Phys B34

http://www2.ece.ohio-state.edu/~lu/ECE331_Wi06_lec_10.pdf. Last retrieved 3. October 2021

Jellison GE (1992) Optical functions of GaAs, GaP, and Ge determined by two-channel polarization modulation ellipsometry. Opt Mater 1:151–160. https://doi.org/10.1016/0925-3467(92)90022-F0

Kemei SK, Kirui MSK, Ndiritu, FG, Odhiambo PM, Ngumbu RG, Amollo TA (2012) Determination of hall effect parameters of gallium arsenide and gallium manganese arsenide by Van Der Pauw Geometry. Adv Phys Theor Appl, vol 8. ISSN (Online) 2225-0638

Kilgore S, Gaw C, Henry H, Hill D, Schroder D (2005) Electromigration of electroplated gold interconnects. Mater Res Soc Symp Proc. https://doi.org/10.1557/PROC-863-B8.30

Kim KJ, Tadokoro S (2007) Electroactive polymers for robotic applications. Artif Muscles Sens. https://doi.org/10.1007/978-1-84628-372-7

Lacour S, Pelrine R, Wagner S, Prahlad H (2003) Photoconductive high-voltage switches of thin film amorphous silicon for EAP actuators. Proc Int Soc Opt Eng 5051:412–418. https://doi.org/10.1117/12.484712

Langer C, Prommesberger C, Ławrowski R, Schreiner R (2016) Field emission properties of p-type black silicon on pillar structures. J Vac Sci Technol, B 34:02G107. https://doi.org/10.1116/1.4943919

Langer C, Ławrowski R, Prommesberger C, Dams F, Serbun B, Bachmann M, Müller G, Schreiner R (2014) High aspect ratio silicon tip cathodes for application in field emission electron sources. In: Proceedings of 27th international vacuum nanoelectronics conference, pp 222–223

Look DC (1990) Review of hall effect and magnetoresistance measurements in GaAs materials and devices. J Electrochem Soc 137:260–266. https://doi.org/10.1149/1.20863790

Monkman GJ (2000) Workpiece retention during machine processing. assembly automation 20. MCB University Press. https://doi.org/10.1108/01445150110381754

Monkman GJ, Egersdörfer S, Meier A, Böse H, Baumann M, Ermert H, Kahled W, Freimuth H (2003) Technologies for haptic displays in teleoperation. Ind Robot Int J 30:525–530. https://doi.org/10.1108/01439910310506792

Mourou G (1980) Apparatus for switching high voltage pulses with picosecond accuracy. US Patent 4,218,618

Mourou G, Knox W (1979) High power switching with picosecond precision. Appl Phys Lett 35:492. https://doi.org/10.1063/1.91207

Myres WC (1980) Semiconductor high voltage switch. US patent 4,240,088, 16 Dec. 1980

Opto-150: 15kV High Voltage Opto-Coupler. HVM Technology New Braunfels, Texas, USA. https://www.hvmtech.com/opto-150. Accessed 12 Aug 2021

Paschen F (1889) Über die zum Funkenübergang in Luft, Wasserstoff und Kohlensäure bei verschiedenen Drucken erforderliche Potentialdifferenz. Ann Phys 273:69–96. https://doi.org/10.1002/andp.18892730505

Perkin Elmer (2001) Photo conductive cells. Perkin Elmer Optoelectronics

Pesavento (1987) Photoconductive Power Switch. US Patent 4,695,733

Rigden JS (1996) Macmillan encyclopedia of physics. Simon & Schuster Macmillan, New York

Salzberger M, Rutzinger M, Zimmermann CG (2017) Voltage-dependent photocurrent in irradiated GaAs solar cells. Prog Photovoltaics. https://doi.org/10.1002/pip.2983

Solymar L, Walsh D (1993) Lectures on the electrical properties of materials. Oxford University Press. https://inis.iaea.org/search/search.aspx?orig_q=RN:26065836

Sze SM (1981) Physics of semiconductor devices. Wiley-Interscience, New York

Thummala P, Huang L, Zhang Z, Andersen MAE (2012) Analysis of dielectric electro active polymer actuator and its high voltage driving circuits. In: IEEE proceedings of the international power modulator symposium and high voltage workshop. https//doi.org/https://doi.org/10.1109/IPMHVC.2012.6518779

Tipler PA, Llewellyn RA (1999) Modern physics, 3rd Ed., W.H. Freeman

Viana ER, Ribeiro GM, de Oliveira AG, Peres ML, Rubinger RM, Rubinger CPL (2012) Antilocalization effect on photo-generated carriers in semi-insulating GaAs sample. Mater Res 15:530–535. https://doi.org/10.1590/S1516-14392012005000065

Waanders JW (1991) Piezoelectric ceramics. Philips Components, Eindhoven

Wang E-D, Kewisch J, Jain A, Ben-Zvi I, Gupta R, Burrill A, Holmes D, Rao T, Zhao K (2011) Heat load of a GaAs photocathode in an SRF electron gun. Chin Phys C 35:387–391

Wiener M, Bovino LJ, Burke T, Kim AH (1989) High energy optically controlled kilovolt semiconductor switch. US Statutory Invention Registration H695–3

Wolfson R, Pasachoff JM (1999) Physics. Addison Wesley Longman, Reading MA

Zappa O, Monkman GJ, Egersdörfer S, Datzer G, Kahled W, Böse H, Tunayer A (2004) High voltage switching using bulk GaAs. Proc. Actuator'04, Bremen

Zhu R, Wallrabe U, Wapler MC, Woias P, Mescheder U (2016) Dielectric electroactive polymer membrane actuator with ring-type electrode as driving component of a tactile actuator. Proc. 30th Eurosensors Conference. 168:1537–1540. https://doi.org/10.1016/j.proeng.2016.11.455